

Monopole-Skyrmions

B. Kleihaus[†], D. H. Tchrakian^{†*} and F. Zimmerschied[†]

[†]Department of Mathematical Physics, National University of Ireland Maynooth,
Maynooth, Ireland

^{*}School of Theoretical Physics – DIAS, 10 Burlington Road, Dublin 4, Ireland

Abstract

A systematic numerical study of the classical solutions to the combined system consisting of the Georgi-Glashow model and the $SO(3)$ gauged Skyrme model is presented. The gauging of the Skyrme system permits a lower bound on the energy, so that the solutions of the composite system can be topologically stable. The solutions feature some very interesting bifurcation patterns, and it is found that some branches of these solutions are unstable.

1 Introduction

The physical motivation of the present work is to set the framework for a semiclassical approach to describing the mechanism of monopole catalysis of Baryon number decay, proposed by Rubakov [1] and Callan [2]. Here we are led by the work of Callan and Witten [3], where the Baryon is described as the soliton of the Skyrme [4] model, in the background of the $U(1)$ Maxwell field of a monopole in the Dirac gauge. In the present work, the Baryon is again described by a Skyrmion, which in this case interacts with the full $SO(3)$ non-Abelian Higgs model (the Georgi-Glashow model) so that the Skyrmion we consider is gauged with the full $SO(3)$ group and interacts with the 't Hooft-Polyakov monopole [5]. We will refer to this model as Monopole-Skyrmion model (MSM).

The most important difference between the present work and that of Ref. [3] is that here we have *two* distinct topological charges - the first being the Baryon number of the Skyrmion and the second, the monopole charge. The energy of our composite system therefore has a topological lower bound consisting of a combination of these two charges of rather different geometric natures, the Baryon charge being a *degree* which cannot be expressed as a total divergence while the monopole charge is a *flux* by virtue of being descended from the second Chern-Pontryagin class.

The most important feature of describing the interaction of the Skyrmion with the gauge field in our Monopole-Skyrmion model is the prescription of gauging the Skyrme field with the diagonal $SU(2)$. This prescription was introduced in Ref. [6] for the gauged Skyrme model, where no Higgs field and Higgs potential are present, and the resulting solutions were studied in Ref. [7, 8]. Most importantly, this gauging permits a lower bound on the energy of the gauged Skyrmion unlike in the case when the usual gauging is from the left, e.g. in Ref. [11] where there is no lower bound. In this paper, we shall refer to the models arising from the gauging prescription used in [6] as gauged Skyrme models (GSM). Since the topological lower bounds for the GSMs were presented in detail in Refs. [6, 7], and because all that we need to know here is that these exist, we do not discuss them further here.

Now the presence of a topological lower bound is not a sufficient condition for the existence of a topologically stable soliton. To illustrate this we refer to the graph of the energy versus Skyrme coupling constant in Fig. 1 for the GSM studied in [7, 8]. Without being mathematically rigorous one can suppose that the branches A_{gs} and B_{gs} correspond to solutions, which form local minima of the energy functional, whereas the connecting branch \tilde{A}_{gs} correspond to solutions, which form saddlepoints.

The bifurcation structure in Fig. 1 is quite different from that appearing in models where the Skyrme field is gauged as in [11] without a topological lower bound. The corresponding graph to Fig. 1 in that case is given in the work of Ref. [12] featuring only two branches as opposed to the three in Fig. 1. Of these two branches [12] only one corresponds to stable solutions, as expected from the work of Refs. [13]. Thus a butterfly pattern of bifurcations with two stable branches seems to be typical of GSMs with topological lower bounds. We will find in our study of the Monopole-Skyrme model, that the butterfly of Fig. 1 persists for some range of the parameters in the model.

Having already presented the lower bound on the energy of Monopole-Skyrme model in Ref. [8], we do not repeat it here and proceed straight away to the study the solutions numerically,

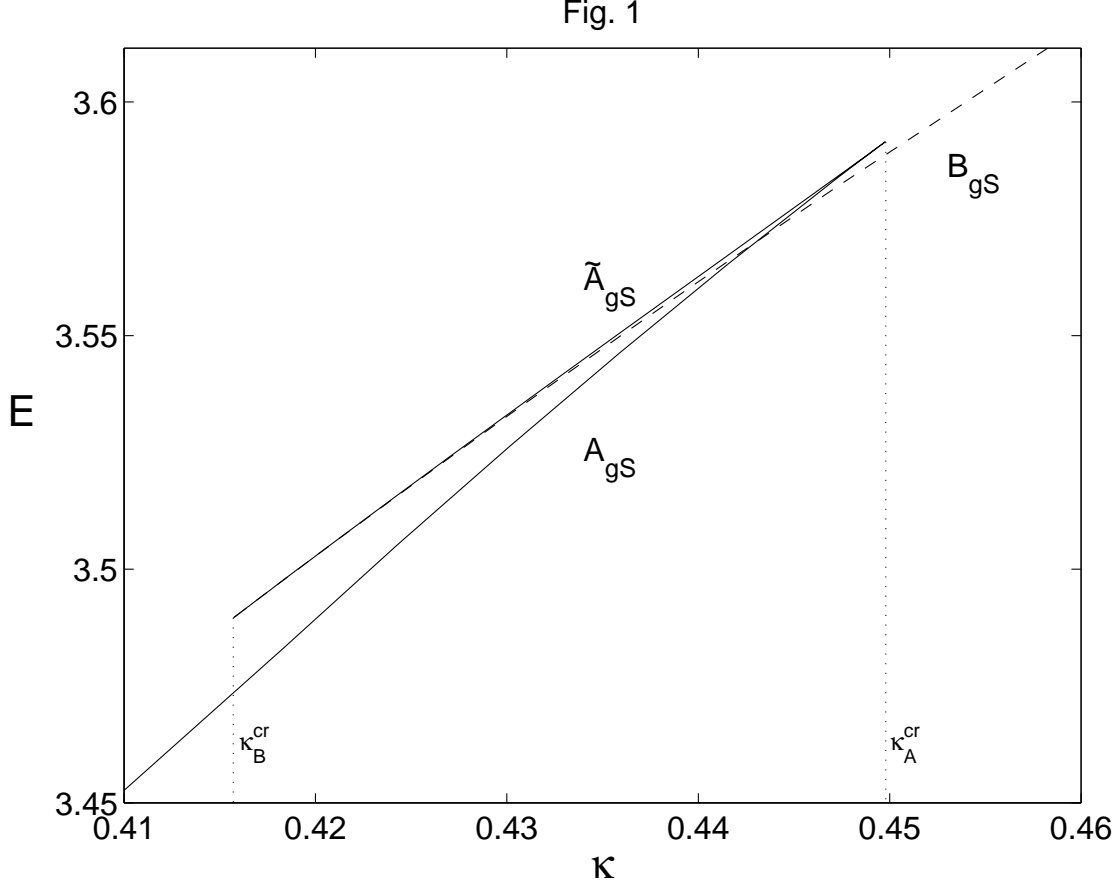


Figure 1: The energy of the gauged Skyrmion as a function of κ in the region of the bifurcation.

with a view to exposing some of their qualitative features that may be of some physical interest. The model we employ here is a slightly modified version of the one in Ref. [8]. It features a particular interaction term between the Higgs field and the chiral field in such a way that it also fixes the asymptotic values of the chiral field subject to the finite energy condition, and assuring integral Baryon number. In Section 2 we present the model, discuss its spectrum, and discuss some scaling properties which will become pivotal in the subsequent numerical analysis. In Section 3, we subject the system to spherical symmetry and give the classical equations to be integrated, the detailed numerical results of which we give in Section 4. In Section 5 we analyse the normal modes of the radial fluctuations around the solutions to the MSM, characterised by those values of the parameters for which the solutions display butterfly bifurcations, and verify that indeed the branches corresponding to \tilde{A}_{gS} are unstable. A summary and discussions of our results are given in Section 6.

2 The Model

The Lagrangian of the Monopole-Skyrme model is given by

$$\begin{aligned}
-\mathcal{L}[A, \Phi, U] = & \int \left(\frac{1}{2g^2} \text{Tr} \{F_{\mu\nu} F^{\mu\nu}\} + \frac{1}{4} \text{Tr} \{D_\mu \Phi D^\mu \Phi\} + \frac{\tilde{\lambda}}{2} \text{Tr} \{(\Phi^2 - \eta^2)^2\} \right. \\
& - \frac{f_\pi^2}{4} \text{Tr} \{D_\mu U U^\dagger D^\mu U U^\dagger\} - \frac{\tilde{\kappa}^2}{8} \text{Tr} \{[D_\mu U U^\dagger, D_\nu U U^\dagger] [D^\mu U U^\dagger, D^\nu U U^\dagger]\} \\
& \left. + V(\Phi, U) \right) d^3r
\end{aligned} \tag{1}$$

with

$$V(\Phi, U) = \frac{\tilde{g}_{\pi\Phi}^2 f_\pi^2}{4} \text{Tr} \left\{ \Phi^2 - \left[\frac{1}{4} (\{\Phi, U\} + \{\Phi, U^\dagger\}) \right]^2 \right\}. \tag{2}$$

The field strength tensor of the $su(2)$ gauge potential $A_\mu = A_\mu^a \frac{\tau_a}{2}$ is defined as

$$F_{\mu\nu} = \partial_\mu A_\nu - \partial_\nu A_\mu + i[A_\mu, A_\nu], \tag{3}$$

and the covariant derivatives for the Higgs field $\Phi = \phi^a \tau_a$ and the chiral matrix $U = \exp\{i\pi^a \tau_a\}$ are defined as

$$D_\mu \Phi = \partial_\mu \Phi + i[A_\mu, \Phi], \tag{4}$$

$$D_\mu U = \partial_\mu U + i[A_\mu, U], \tag{5}$$

respectively. g denotes the gauge coupling parameter, λ the strength of the Higgs potential, η the norm of the vacuum expectation value of the Higgs field, f_π the pion decay constant and κ the Skyrme coupling parameter. The parameter $g_{\pi\Phi}$ characterises the direct coupling between the Higgs boson and the chiral matrix.

The first three terms in (1) are the familiar Georgi-Glashow model which is characterised by the scale η . The next two terms are the Skyrme model with covariant derivatives $D_\mu U$ allowing for an interaction of the chiral matrix with the gauge potential. The first of these terms introduces another scale, f_π . The last term $V(\Phi, U)$ describes a direct coupling of the chiral matrix with the Higgs field, on which we will comment later.

The Lagrangian (1) is invariant under local $SU(2)$ gauge transformations \mathbf{g} ,

$$\begin{aligned}
A_\mu & \longrightarrow \mathbf{g} A_\mu \mathbf{g}^{-1} + i \partial_\mu \mathbf{g} \mathbf{g}^{-1}, \\
\Phi & \longrightarrow \mathbf{g} \Phi \mathbf{g}^{-1}, \\
U & \longrightarrow \mathbf{g} U \mathbf{g}^{-1}.
\end{aligned}$$

The vacuum of the theory is given by the following constant configuration,

$$A_\mu \equiv 0, \quad \Phi \equiv \eta \tau_3, \quad U \equiv \mathbf{1}. \tag{6}$$

In order to identify the particle content of the model we expand around the vacuum,

$$A_\mu = \delta a_\mu^a \frac{\tau_a}{2}, \quad \Phi = \eta \tau_3 + \delta \phi^a \tau_a, \quad U = \left(\mathbf{1} - \frac{\delta \pi^a \delta \pi^a}{2} \right) + i \delta \pi^a \tau_a, \tag{7}$$

and insert into the equation of motion obtained from the Lagrangian (1). Neglecting quadratic terms in δa_μ^a , $\delta\phi^a$ and $\delta\pi^a$ we find

$$\begin{aligned}\partial_\mu\partial^\mu\delta\pi^a &= \tilde{g}_\pi^2\eta^2\delta\pi^a, \quad a = 1, 2, 3, \\ \partial_\mu\partial^\mu\delta\phi^3 &= 4\tilde{\lambda}\eta^2\delta\phi^3, \\ \partial_\mu\partial^\mu\delta a^{\nu,3} &= 0, \\ \partial_\mu\partial^\mu\delta\bar{a}^{\nu,a} &= g^2\eta^2\delta\bar{a}^{\nu,a}, \quad a = 1, 2, \end{aligned}$$

where we have defined $\delta\bar{a}_\mu^a = \delta a_\mu^a + \frac{1}{\eta}\partial_\mu\delta\phi^b\epsilon_{a3b}$, and used the gauge fixing conditions $\partial_\mu\delta a^{\mu,3} = 0$ and $\partial_\mu\delta\bar{a}^{\mu,a} = 0$ for $a = 1, 2$. Thus we find for the masses of the gauge field, the chiral field and the Higgs field,

$$m_A = g\eta, \quad m_\pi = \tilde{g}_{\pi\Phi}\eta, \quad m_h = 2\sqrt{\tilde{\lambda}}\eta, \quad (8)$$

respectively. (We take all parameters $g, \tilde{g}_{\pi\Phi}, \eta, \tilde{\lambda}$ to be positive). Clearly, the mass of the chiral field stems from the interaction term of the chiral matrix with the Higgs field, which breaks the chiral symmetry. However, the spontaneous symmetry breaking does not lead to a mass splitting for the chiral fields.

In the following we will motivate the potential term (2) for the Higgs field and the chiral matrix. First consider the model without the potential term. From the finite energy conditions we find for the chiral field and the Higgs field in the limit $r \rightarrow \infty$

$$D_\mu\Phi \rightarrow 0, \quad D_\mu U \rightarrow 0. \quad (9)$$

Let us assume, that this condition is fulfilled for the radial component of the covariant derivatives and concentrate on the angular components. We decompose the Higgs field and the chiral matrix in the form

$$\begin{aligned}\Phi &= h\hat{\phi}, \quad \hat{\phi} = \hat{\phi}^a\tau_a, \quad \text{with } \hat{\phi}^a\hat{\phi}^a = 1, \\ U_\infty &= \cos f\mathbf{1} + i\sin f\hat{u}, \quad \hat{u} = \hat{u}^a\tau_a, \quad \text{with } \hat{u}^a\hat{u}^a = 1, \end{aligned} \quad (10)$$

respectively, where $h, \hat{\phi}^a$ and f, \hat{u}^a are functions of the variables r, θ, φ .

From the finite energy conditions follows that at infinity $|h| = \eta, f_\infty = \text{const.}$ However, $\hat{\phi}^a$ and \hat{u}^a may still be functions of the angular variables θ, φ . The conditions (9) now become

$$D_\alpha\Phi_\infty = (\partial_\alpha\hat{\phi} + i[A_\alpha, \hat{\phi}])|_\infty = 0, \quad D_\alpha U_\infty = \sin f_\infty (\partial_\alpha\hat{u} + i[A_\alpha, \hat{u}])|_\infty = 0, \quad (11)$$

where $\alpha = \theta, \varphi$. The first condition can be fulfilled with $A_\alpha|_\infty = \left(\frac{i}{2}\partial_\alpha\hat{\phi}\hat{\phi} + A_\alpha^{(\phi)}\hat{\phi}\right)|_\infty$, where $A_\alpha^{(\phi)}$ is some function of θ, φ . The second condition can be fulfilled either with $f_\infty = 0$ or with $A_\alpha|_\infty = \left(\frac{i}{2}\partial_\alpha\hat{u}\hat{u} + A_\alpha^{(u)}\hat{u}\right)|_\infty$, where $A_\alpha^{(u)}$ is again some function of θ, φ . If the latter condition is fulfilled, f_∞ may take arbitrary values. Hence, these configurations can be deformed continuously into configurations with trivial chiral matrix.

In order to avoid this problem we have introduced the potential (2) into the Lagrangian. Using the general decomposition (10) the potential can be written as $V(\Phi, U) = \frac{1}{2}\tilde{g}_{\pi\Phi}^2 f_\pi^2 h^2 \sin^2 f$,

i. e. it couples the modulus of the Higgs field $|h|$ and the chiral function f , and does not depend on the “phases” $\hat{\phi}^a, \hat{u}^a$. Consequently, the masses for the chiral fields, introduced by the potential at infinity, do not depend on the direction of the Higgs field in isospace. Furthermore, the finite energy condition now forces $f_\infty = n\pi$, where n is an integer.

The sum of the potentials in (1) has global minima at $|h| = \eta, f = n\pi$, and the matrix of the second variations has only non-negative eigenvalues at the global minima, provided the parameters λ and $\tilde{g}_{\pi\Phi}^2$ are positive.

In order to study the consequences of the two scales f_π and η we will take two points of view. First we will fix f_π and express all dimensionful quantities in units of f_π . Equivalently, we can fix η and express all dimensionful quantities in units of η . In each case, the ratio of the scales will enter the equations of motion as a parameter.

We define the dimensionless quantities $x = rf_\pi g$, $\hat{\Phi} = \Phi/f_\pi$, $\eta_0 = \eta/f_\pi$. Then the Hamiltonian becomes

$$\begin{aligned} \mathcal{H}[A, \hat{\Phi}, U] = & \frac{f_\pi}{g} \int \left(\frac{1}{2} \text{Tr} \{F_{\mu\nu} F^{\mu\nu}\} + \frac{1}{4} \text{Tr} \{D_\mu \hat{\Phi} D^\mu \hat{\Phi}\} + \frac{\lambda}{2} \text{Tr} \{(\hat{\Phi}^2 - \eta_0^2)^2\} \right. \\ & - \frac{1}{4} \text{Tr} \{D_\mu U U^\dagger D^\mu U U^\dagger\} - \frac{\kappa^2}{8} \text{Tr} \{[D_\mu U U^\dagger, D_\nu U U^\dagger] [D^\mu U U^\dagger, D^\nu U U^\dagger]\} \\ & \left. + \frac{\tilde{g}_{\pi\Phi}^2}{4} \text{Tr} \left\{ \hat{\Phi}^2 - \left[\frac{1}{4} (\{\hat{\Phi}, U\} + \{\hat{\Phi}, U^\dagger\}) \right]^2 \right\} \right) d^3x, \end{aligned} \quad (12)$$

where we have defined $\lambda = \tilde{\lambda}/g^2$, $\kappa = \tilde{\kappa}g$, $g_{\pi\Phi} = \tilde{g}_{\pi\Phi}/g$. In terms of masses Eq. (8) the parameters $g_{\pi\Phi}$ and λ can be expressed as $g_{\pi\Phi} = m_\pi/m_A$ and $\sqrt{\lambda} = 2m_h/m_A$, respectively. The parameter $\eta_0 = f_\pi/\eta$ denotes the ratio of the scales. Apart from the last term the Hamiltonian (12) this is equivalent to the Hamiltonian studied before in [8]. The difference is, that we now consider η_0 as a free parameter. In the limit $\eta_0 \rightarrow 0$ the minimum of the Higgs potential allows for a vanishing Higgs field. In this case we find the gauged Skyrme model considered before in [6, 7, 8].

Fixing the scale parameter η we define $\bar{x} = \eta gr$, $\bar{\Phi} = \eta\Phi$ and $\xi = f_\pi/\eta$. Then the Hamiltonian becomes

$$\begin{aligned} \mathcal{H}[A, \bar{\Phi}, U] = & \frac{\eta}{g} \int \left(\frac{1}{2} \text{Tr} \{F_{\mu\nu} F^{\mu\nu}\} + \frac{1}{4} \text{Tr} \{D_\mu \bar{\Phi} D^\mu \bar{\Phi}\} + \frac{\bar{\lambda}}{2} \text{Tr} \{(\bar{\Phi}^2 - 1)^2\} \right. \\ & - \frac{\xi^2}{4} \text{Tr} \{D_\mu U U^\dagger D^\mu U U^\dagger\} - \frac{\bar{\kappa}^2}{8} \text{Tr} \{[D_\mu U U^\dagger, D_\nu U U^\dagger] [D^\mu U U^\dagger, D^\nu U U^\dagger]\} \\ & \left. + \frac{\bar{g}_{\pi\Phi}^2 \xi^2}{4} \text{Tr} \left\{ \bar{\Phi}^2 - \left[\frac{1}{4} (\{\bar{\Phi}, U\} + \{\bar{\Phi}, U^\dagger\}) \right]^2 \right\} \right) d^3\bar{x}, \end{aligned} \quad (13)$$

with $\bar{\lambda} = \tilde{\lambda}/g^2 = \lambda$, $\bar{\kappa} = \tilde{\kappa}g = \kappa$ and $\bar{g}_{\pi\Phi} = \tilde{g}_{\pi\Phi}/g = g_{\pi\Phi}$.

Comparing with the case of fixed scale f_π we find $\xi = 1/\eta_0$, $\bar{x} = \eta_0 x$, $\bar{\Phi} = \hat{\Phi}/\eta_0$. Because the Hamiltonians (12) and (13) are equivalent, we can obtain the properties of (12) from (13) and vice versa by using these relations. In particular, for the dimensionless energies $E \equiv \frac{g}{4\pi f_\pi} \mathcal{H}$ and

$\bar{E} \equiv \frac{g}{4\pi\eta} \mathcal{H}$ we have $\bar{E} = \frac{E}{\eta_0}$. We will opt to work with (12) in the following.

3 Static spherically symmetric equations

The static spherically symmetric, purely magnetic Ansatz for the gauge field is [9, 10]

$$A_0 = 0, A_r = c(x) \frac{\tau_r}{2}, A_\theta = (1 - a(x)) \frac{\tau_\varphi}{2} + b(x) \frac{\tau_\theta}{2}, A_\varphi = -\sin \theta \left((1 - a(x)) \frac{\tau_\theta}{2} - b(x) \frac{\tau_\varphi}{2} \right), \quad (14)$$

where the $su(2)$ matrices τ_α , $\alpha = r, \theta, \varphi$ are defined in terms of the Pauli matrices τ_1, τ_2, τ_3 by

$$\begin{aligned} \tau_r &= \sin \theta (\cos \varphi \tau_1 + \sin \varphi \tau_2) + \cos \theta \tau_3, \\ \tau_\theta &= \cos \theta (\cos \varphi \tau_1 + \sin \varphi \tau_2) - \sin \theta \tau_3, \\ \tau_\varphi &= -\sin \varphi \tau_1 + \cos \varphi \tau_2. \end{aligned}$$

The spherically symmetric Ansatz for the Higgs field is

$$\hat{\Phi} = h(x) \tau_r, \quad (15)$$

and for the chiral matrix

$$U = \cos f(x) + i \sin f(x) \tau_r. \quad (16)$$

The Ansatz is form invariant under the $U(1)$ gauge transformations [9]

$$\mathbf{g} = \exp \left\{ i \frac{\Gamma}{2} \tau_r \right\}, \quad (17)$$

where the gauge transformation function Γ is an arbitrary function of x . The gauge field functions transform as

$$\begin{aligned} c(x) &\rightarrow c(x) - x \Gamma'(x), \\ b(x) &\rightarrow \cos \Gamma(x) b(x) - \sin \Gamma(x) a(x), \\ a(x) &\rightarrow \cos \Gamma(x) a(x) + \sin \Gamma(x) b(x), \end{aligned} \quad (18)$$

whereas the Higgs field function $h(x)$ and the chiral function $f(x)$ are invariant. To fix this gauge freedom we first impose the condition $c(x) \equiv 0$, which still allows for global transformations with $\Gamma = \text{const}$. Further, we find that the functions $a(x)$ and $b(x)$ enter the Lagrangian only in the form $a'^2(x) + b'^2(x)$ and $a^2(x) + b^2(x)$, which permits us to set $b(x) \equiv 0$.

With the Ansatz (14)-(16) restricted to the gauge fixing conditions and $b(x) \equiv 0$ the Hamiltonian (12) becomes

$$\begin{aligned} \mathcal{H}[a, h, f] &= \frac{4\pi f_\pi}{g} \int \left(a'^2 + \frac{(a^2 - 1)^2}{2x^2} + \frac{x^2 h'^2}{2} + a^2 h^2 + \lambda (h^2 - \eta_0^2)^2 x^2 \right. \\ &\quad \left. + \frac{x^2 f'^2}{2} + a^2 \sin^2 f + 4\kappa^2 a^2 \sin^2 f (f'^2 + \frac{a^2 \sin^2 f}{2x^2}) \right. \\ &\quad \left. + \frac{g_{\pi\Phi}^2 x^2}{2} h^2 \sin^2 f \right) dx. \end{aligned} \quad (19)$$

The differential equations for the functions $a(x)$, $h(x)$ and $f(x)$ can now be obtained as the variational equations which extremize the Hamiltonian (19),

$$\begin{aligned}
a'' &= a \left\{ \frac{(a^2 - 1)}{x^2} + h^2 + \sin^2 f \left[1 + 4\kappa^2 (f'^2 + \frac{a^2 \sin^2 f}{x^2}) \right] \right\} , \\
h'' &= -2 \frac{h'}{x} + h \left\{ 2 \frac{a^2}{x^2} + 4\lambda(h^2 - \eta_0^2) + g_{\pi\Phi}^2 \sin^2 f \right\} , \\
f'' &= \left\{ 8\kappa^2 a \sin f \left[a \cos f \left(\frac{a^2 \sin^2 f}{x^2} - f'^2 \right) - 2 \sin f a' f' \right] + 2(\sin f \cos f a^2 - x f') \right. \\
&\quad \left. + g_{\pi\Phi}^2 \sin f \cos f h^2 x^2 \right\} \frac{1}{x^2 + 8\kappa^2 a^2 \sin^2 f} .
\end{aligned} \tag{20}$$

These equations have to be solved due to boundary conditions which ensure regularity of the solution at the origin and finite energy, i. e.

$$\begin{aligned}
x = 0 & : a = 1 , \quad h = 0 , \quad f = \pi , \\
x \rightarrow \infty & : a \rightarrow 0 , \quad h \rightarrow \eta_0 , \quad f \rightarrow 0 .
\end{aligned} \tag{21}$$

4 Numerical results

We have constructed numerically solutions of the model for several values of the parameters η_0 , λ , κ and $g_{\pi\Phi}$. In particular we investigated the dependence of the solutions on the parameters η_0 and κ .

In Figs. 2a and 2b we show the energy $E = \frac{g}{4\pi f_\pi} \mathcal{H}$ as a function of η_0 for several values of κ for $\lambda = 0$ and $g_{\pi\Phi} = 0$. For large values of η_0 the energy is a monotonically increasing function of η_0 . In the limit $\eta_0 \rightarrow \infty$ the energy increases linearly with η_0 , such that $E/\eta_0 \rightarrow 1$, i. e. the energy becomes equal to the Monopole energy (in units of $4\pi\eta$). Indeed, this limit corresponds to the limit $f_\pi \rightarrow 0$ where the chiral field becomes trivial, $U = -1$ everywhere except at infinity.

4.1 $\eta \ll f_\pi$

For small values of η_0 the solutions develop bifurcations, corresponding to the ‘butterfly’ structures in Fig. 2a, where for a fixed value of η_0 three solutions coexist. We observe from Fig. 2a that the bifurcations occur only for a finite range of the parameter κ , $\kappa_{\text{cr}}^{(1)} < \kappa < \kappa_{\text{cr}}^{(2)}$, where $\kappa_{\text{cr}}^{(1)}, \kappa_{\text{cr}}^{(2)}$ depend on λ and $g_{\pi\Phi}$. For $\lambda = 0$, $g_{\pi\Phi} = 0$ we find $\kappa_{\text{cr}}^{(1)} \approx 0.374$ and $\kappa_{\text{cr}}^{(2)} \approx 0.4495$. We demonstrate the details of the bifurcations in Fig. 2b for $\kappa = 0.4$ as an example. This figure suggests that the branches B and A correspond to local minima of the energy functional, whereas the branch \tilde{A} corresponds to saddlepoint solutions.

The bifurcation pattern looks similar to the bifurcation pattern found recently in the gauged Skyrme model [8]. Indeed, the bifurcations in the Monopole-Skyrme model and the gauged Skyrme model are closely related to each other. In the limit $\eta_0 \rightarrow 0$ the Higgs potential allows for a vanishing Higgs field. In this case we obtain the gauged Skyrmion model studied in Refs. [6,

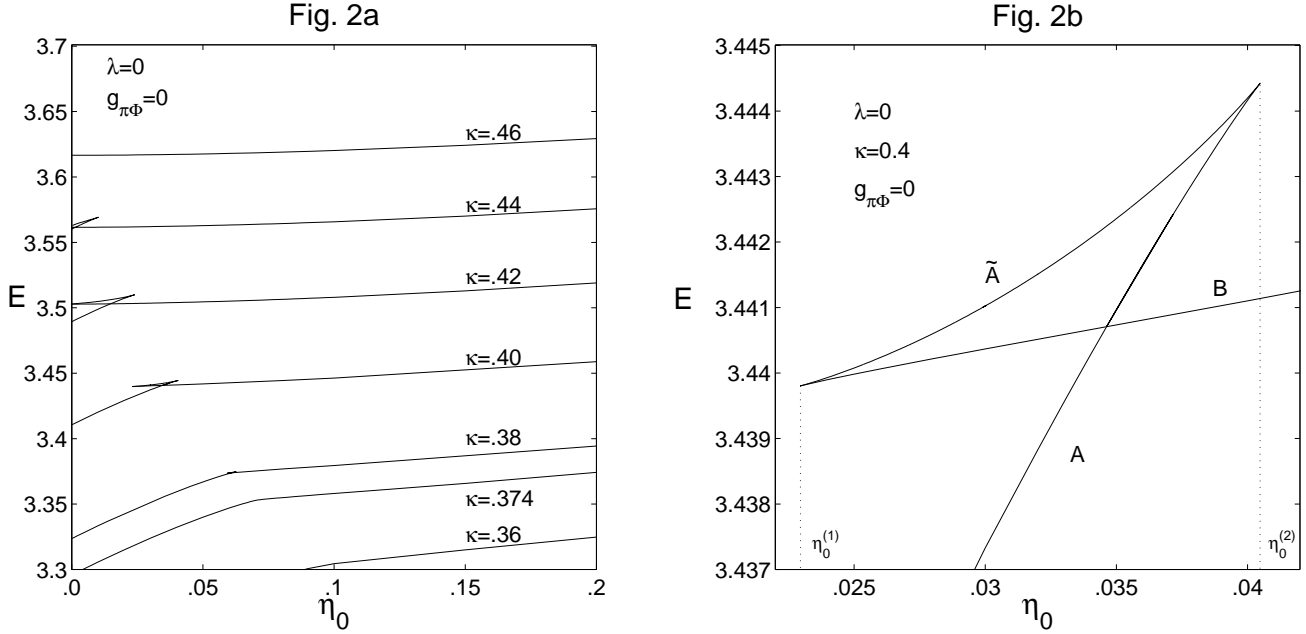


Figure 2: (a) The dimensionless energy of the Monopole-Skyrmion solutions is shown as a function of η_0 for several values of κ for fixed $\lambda = 0$ and $g_{\pi\Phi} = 0$. (b) The same as (a) for fixed $\kappa = 0.4$, $\lambda = 0$ and $g_{\pi\Phi} = 0$. $\eta_0^{(1)}$ and $\eta_0^{(2)}$ indicate the values of η_0 where the branches B and A merge with the saddlepoint branch \tilde{A} , respectively.

7, 8]. Consequently, the Monopole-Skyrmion solutions should approach the gauged Skyrmion solution in the limit of vanishing η_0 . In Fig. 3 we show in a 3D graph the energy of the Monopole-Skyrmion solutions as a function of η_0 and κ together with the energy of the gauged Skyrmion solutions. We observe, that indeed the energy of the Monopole-Skyrmion coincides with the energy of the gauged Skyrmion in the limit $\eta_0 \rightarrow 0$.

In order to understand the behaviour of the solutions for small η_0 , let us first discuss the solutions of the Higgs-less gauged-Skyrme model. In this model the absence of the Higgs field allows two possibilities for the value of the gauge field function $a(x)$ at infinity. For large values of κ the function $a(x)$ vanishes at infinity (branch B_{gs}) whereas for small values of κ the function $a(r)$ approaches the value one at infinity (branches A_{gs} and \tilde{A}_{gs}). These two cases correspond to the dashed and solid lines, respectively, plotted in the $E - \kappa$ plane in Fig. 3. For a certain range of values $\kappa_B^{cr} < \kappa < \kappa_A^{cr}$ three branches of solutions are present, reminding one of two local minima (B_{gs} and A_{gs}) and a saddlepoint (\tilde{A}_{gs}) of the energy functional.

Now consider the limit $\eta_0 \rightarrow 0$ for the Monopole-Skyrmion solutions. If $\kappa < \kappa_B^{cr}$ the Monopole-Skyrmion solution will approach the unique gauged Skyrmion solution represented by the solid line in Fig. 3, below κ_B^{cr} . However, if $\kappa_B^{cr} < \kappa < \kappa_A^{cr}$ there are three different gauged Skyrmion solutions available. In this case each Monopole-Skyrmion solutions of the branches A , \tilde{A} and B approaches the corresponding gauged Skyrmion solution on the branches A_{gs} , \tilde{A}_{gs} and B_{gs} ,

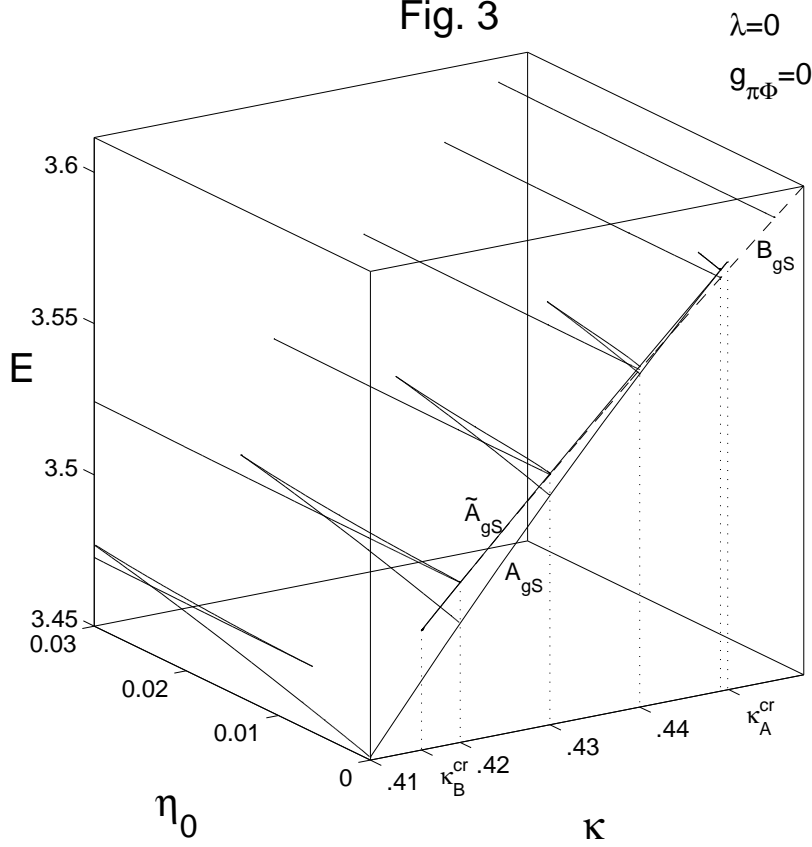


Figure 3: The dimensionless energy of the Monopole-Skyrmion solutions is shown as a function of η_0 for several values of κ for fixed $\lambda = 0$ and $g_{\pi\Phi} = 0$ together with the dimensionless energy of the gauged Skyrmion solutions as a function of κ . κ_B^{cr} and κ_A^{cr} indicate the values of κ where the branches B_{gs} and A_{gs} merge with the branch \tilde{A}_{gs} , respectively.

respectively. For $\kappa > \kappa_A^{cr}$ the Monopole-Skyrmion solutions on the branches A and \tilde{A} Monopole-Skyrmion solutions cease to exist and the solutions on the remaining branch B tend uniquely to the gauged-Skyrmion (B_{gs}) solutions represented by the dashed line above κ_A^{cr} in Fig. 3.

The limit $\eta_0 \rightarrow 0$ is non-uniform for $\kappa < \kappa_A^{cr}$ for the Monopole-Skyrmion solutions on the branches A and \tilde{A} . This is expected because the asymptotic values of the gauge field function $a(x)$ for the Monopole-Skyrmion solutions and the gauged-Skyrmion solutions (branches A_{gs} and \tilde{A}_{gs}) are different. For the latter the function $a(x)$ approaches the value one at infinity, whereas for the former ones $a(x)$ vanishes at infinity. To illustrate the limit $\eta_0 \rightarrow 0$ for small values of κ we exhibit in Figs. 3a-3c as an example a sequence of field configurations of Monopole-Skyrmion solutions along the “butterfly” for $\kappa = 0.4$ in Figs. 2a and 2b. We follow the branch B down to $\eta_0^{(1)}$ (see Fig. 2b), continue with increasing η_0 on the saddlepoint branch \tilde{A} up to $\eta_0^{(2)}$ and finally we approach $\eta_0 = 0$ on the branch A .

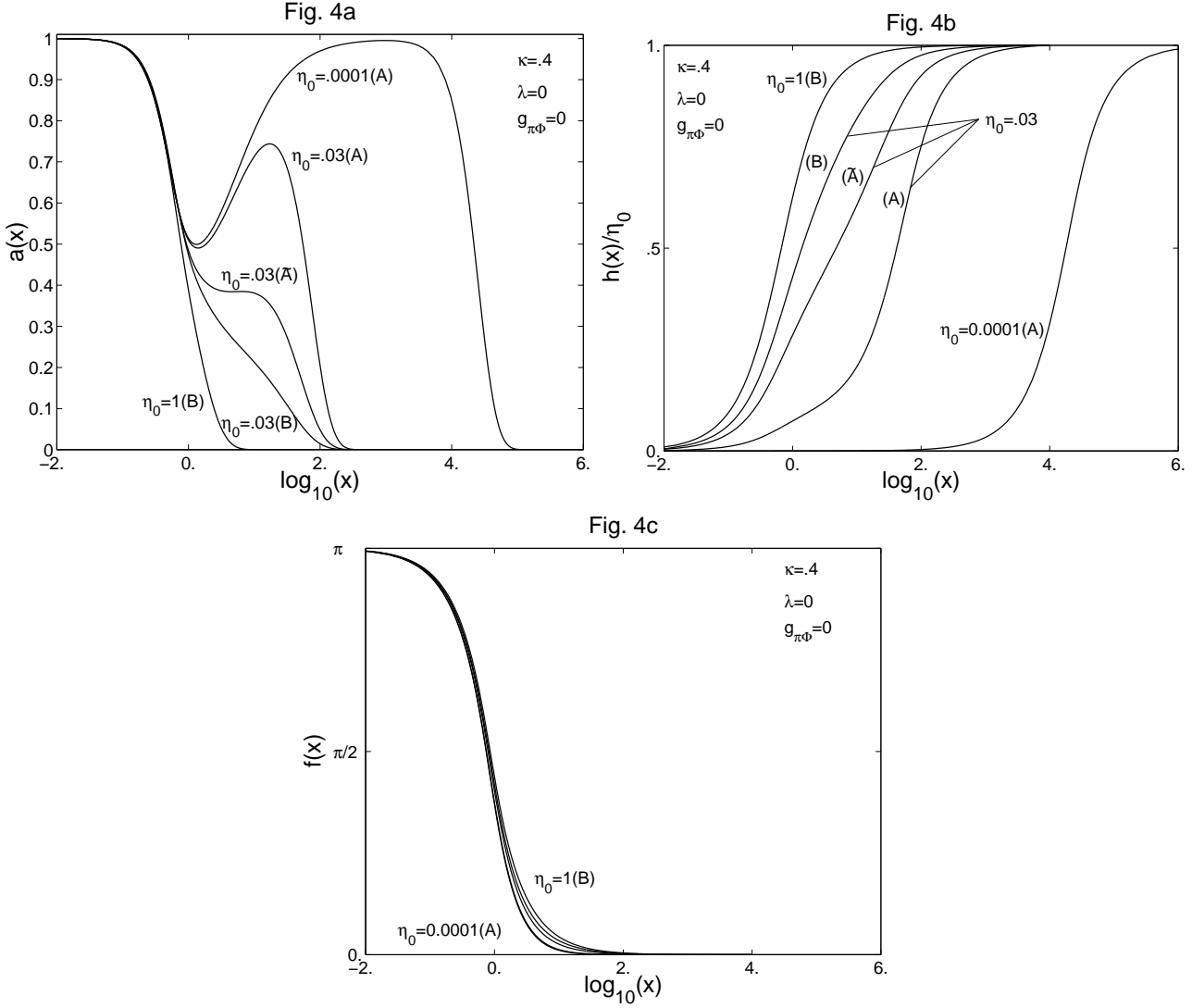


Figure 4: (a) The gauge field function $a(x)$ is shown for several values of η_0 for fixed $\kappa = 0.4$, $\lambda = 0$ and $g_{\pi\Phi} = 0$. (b) The same as Fig. 4a for the scaled Higgs field function $h(x)/\eta_0$. (c) The same as Fig. 4a for the chiral function $f(x)$. The different lines correspond to $\eta_0 = 1(B)$, $\eta_0 = 0.03(B)$, $\eta_0 = 0.03(\tilde{A})$, $\eta_0 = 0.03(A)$ and $\eta_0 = 0.0001(A)$ from top to bottom.

In Fig. 4a the profile of the gauge field function $a(x)$ is shown for $\eta_0 = 1.0$ and $\eta_0 = 0.03$ on branch B , for $\eta_0 = 0.03$ on branch \tilde{A} , and, for $\eta_0 = 0.03$ and $\eta_0 = 0.0001$ on branch A . While for $\eta_0 = 1.0$, $\eta_0 = 0.03(B)$, and $\eta_0 = 0.03(\tilde{A})$, $a(x)$ is a monotonically decreasing function of x , it develops a local maximum at some stage on the branch \tilde{A} while η_0 increases. Passing to the branch A , now with decreasing η_0 , this local maximum persists. Along this path the local maximum $a(x_{\max})$ and its location x_{\max} increase and reach $a(x_{\max} = \infty) = 1$ as η_0 tends to zero,

while the asymptotic region, where $a(x)$ decays to zero, is shifted to infinity. Thus, in the limit $\eta_0 \rightarrow 0$ the gauge field function of the Monopole-Skyrmion solution tends to the corresponding function of the gauged Skyrmion solution for all x *except* at infinity. Therefore the convergence of the Monopole-Skyrmion on A and \tilde{A} to the gauged-Skyrmion solutions on A_{gs} and \tilde{A}_{gs} is *non-uniform*.

In Fig. 4b we exhibit the profiles of the scaled Higgs function $h(x)/\eta_0$ for the same parameters η_0 like in Fig. 4a. We observe that $h(x)/\eta_0$ is a monotonically increasing function of x for all η_0 . However along the path of values of η_0 described above, the magnitudes of the functions $h(x)/\eta_0$ become progressively smaller on an increasing interval, while the asymptotic region, where $h(x)$ approaches its vacuum value η_0 , is shifted to increasing values of x . In the limit $\eta_0 \rightarrow 0$ the function $h(x)$ vanishes everywhere, signaling the merging of the Monopole-Skyrmions to the (Higgs-free) gauged-Skyrmions in this limit.

In Fig. 4c we show the profiles of the chiral function $f(x)$ for the same values of parameters η_0 as in Figs. 4a,b. For all values of η_0 the function $f(x)$ is a monotonically decreasing function of x . In contrast to the gauge field function $a(x)$ and the Higgs field function $h(x)$ the chiral function $f(x)$ does not change considerably with η_0 .

The case discussed above in Figs. 4a,b,c pertains to $\kappa < \kappa_A^{\text{cr}}$. For $\kappa_B^{\text{cr}} < \kappa < \kappa_A^{\text{cr}}$ there are gauged-Skyrmion solutions of both types, namely those on branches A_{gs} and \tilde{A}_{gs} as well as on branch B_{gs} , so the convergence of the Monopole-Skyrmion solutions to the gauged-Skyrmion solutions can be both uniform and non-uniform. In that case the Monopole-Skyrmion solutions on the branches A and \tilde{A} approach the gauged-Skyrmion solutions on the corresponding branches A_{gs} and \tilde{A}_{gs} in a *non-uniform* way, for the same reasons as described above. However, the gauge field function of the Monopole-Skyrmion solutions of the branch B obey the same asymptotic behaviour as the corresponding function of the gauged Skyrmion solutions of the branch B_{gs} . For these solutions the convergence is *uniform*.

For $\kappa > \kappa_A^{\text{cr}}$, there is only one type of gauged-Skyrmion solution, namely those on branch B_{gs} for which the asymptotic value of the gauge field function $a(x)$ equals zero like for the Monopole-Skyrmion solution, and hence the convergence of these solutions as $\eta_0 \rightarrow 0$ is *uniform*.

4.2 $\eta \gg f_\pi$

Let us now consider the case where the scale η is much larger than the scale f_π . In Fig. 5 we show the field configurations for $\eta_0 = 2700$ (solid lines) and for $\eta_0 = 1$ (dashed lines) for comparison. We observe that the gauge field function $a(x)$ for $\eta_0 = 2700$ approaches its asymptotic value at a very small distance from the origin. The same applies to the scaled Higgs field function $h(x)/\eta_0$, except for the long ranged tail, which is due to the power law decay for vanishing Higgs mass, i. e. for $\lambda = 0$. The chiral function $f(x)$, however, extends to larger distances from the origin. This is in contrast to the configuration for $\eta_0 = 1$, where the change in the profile of all functions is roughly on the same interval.

Note, that $\eta_0 = 2700$ corresponds to the case where the parameters f_π and η are of the magnitude of the pion decay constant in low energy QCD and the vacuum expectation value of the Higgs field in the Weinberg-Salam model, respectively. For the energy of this solution we find $4\pi E = 2700.013 \cdot 4\pi$, i. e. roughly the energy of the BPS Monopole ($4\pi\eta$). An appealing

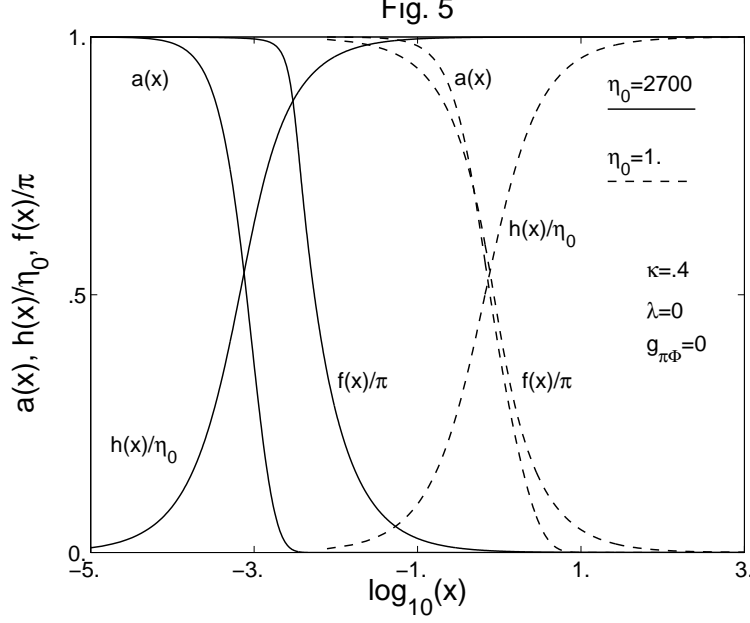


Figure 5: The profiles of the gauge field function $a(x)$, the scaled Higgs field function $h(x)/\eta_0$ and the scaled chiral function $f(x)/\pi$ are shown for $\eta_0 = 2700$ (solid lines) and $\eta_0 = 1$ (dashed lines) for fixed $\kappa = 0.4$, $\lambda = 0$ and $g_{\pi\Phi} = 0$.

physical interpretation of this solution seems to be that a Monopole resides at the center of a baryon and dominates its mass.

This can also be seen in a different way using gauge invariant quantities like topological charges. We define the topological Monopole charge density as

$$\tilde{\rho}_{MP} = \frac{1}{4\pi\eta} \text{Tr} \{ F_{ij} D_k \Phi \} \varepsilon^{ijk} , \quad (22)$$

and according to Ref. [6, 7] the gauge invariant baryonic charge density as

$$\tilde{\rho}_B = \frac{1}{12\pi^2} \left(D_i \xi^a D_j \xi^b D_k \xi^c \xi^d \varepsilon^{abcd} - 3\xi^4 F_{ij}^\alpha D_k \xi^\alpha \right) \varepsilon^{ijk} , \quad (23)$$

where we have defined for $U = \exp(i\pi^\alpha \tau^\alpha)$

$$\xi^4 = \cos |\pi| , \quad \xi^\alpha = \sin |\pi| \frac{\pi^\alpha}{|\pi|} , \quad D_i \xi^\alpha = \partial_i \xi^\alpha + \varepsilon^{\alpha\beta\gamma} A_i^\beta \xi^\gamma , \quad D_i \xi^4 = \partial_i \xi^4 , \quad (24)$$

with a, b, c, d run from 1 to 4 and α, β, γ run from 1 to 3. For the spherically symmetric Ansatz (14-16) and with the dimensionless coordinate x the scaled charge densities become

$$\tilde{\rho}_{MP} = \frac{[h(1-a^2)]'}{4\pi x^2 \eta_0} \quad \text{and} \quad \tilde{\rho}_B = -\frac{[f + (1-2a^2) \sin f \cos f]'}{4\pi^2 x^2} . \quad (25)$$

For $\eta_0 = 0.0001$ and $\eta_0 = 2700$, with fixed $\kappa = 0.4$, $\lambda = 0$, $g_{\pi\Phi} = 0$, we show in Fig. 6 the functions $\rho_{MP} = 4\pi x^2 \tilde{\rho}_{MP}$ (solid lines) and $\rho_B = 4\pi x^2 \tilde{\rho}_B$ (dashed lines) normalized by their respective maxima. The values of the normalization constants are $(4\pi x^2 \tilde{\rho}_{MP})_{\max} = 2.113$ and

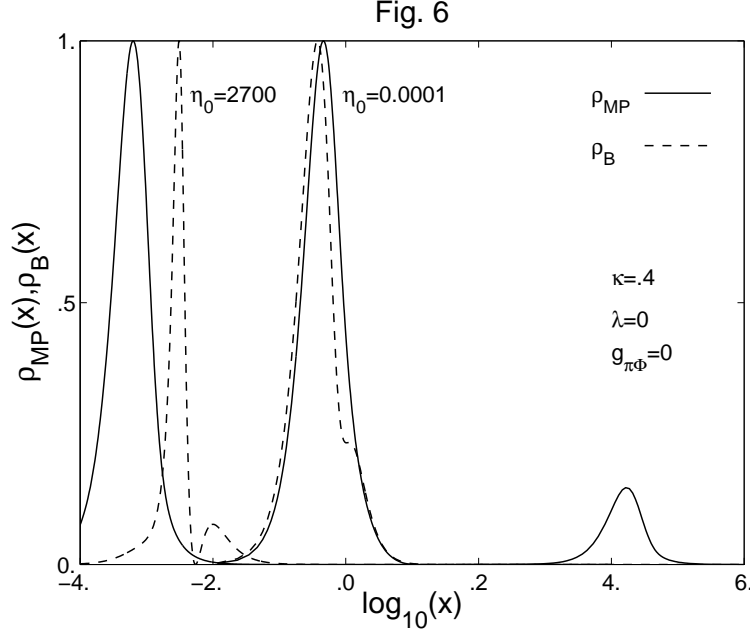


Figure 6: The profiles of the normalized topological functions $\rho_{MP}(x)/\max(\rho_{MP})$ (solid lines) and $\rho_B(x)/\max(\rho_B)$ (dashed lines) are shown for $\eta_0 = 2700$ and $\eta_0 = 0.0001$ for fixed $\kappa = 0.4$, $\lambda = 0$ and $g_{\pi\Phi} = 0$.

$(4\pi x^2 \tilde{\rho}_B)_{\max} = 11080$ for $\eta_0 = 0.0001$, and $(4\pi x^2 \tilde{\rho}_{MP})_{\max} = 0.31$ and $(4\pi x^2 \tilde{\rho}_B)_{\max} = 0.113$ for $\eta_0 = 2700$, respectively.

From Fig. 6 we observe that for $\eta_0 = 2700$ the location x_{\max}^{MP} of the maximum of the function ρ_{MP} resides at a considerably smaller distance from the origin than the location x_{\max}^{B} of the maximum of the function ρ_B . This confirms the interpretation as a Monopole inside a baryon. Note, that the function ρ_B possesses an additional local maximum at a larger distance from the origin than the global maximum and a minimum with vanishing magnitude between the both maxima. We found that half the baryonic charge stems from the area below the first peak and half from the area below the second peak. This can be understood as follows. For distances larger than or near the location of the minimum x_{\min} the gauge field function $a(x)$ almost vanishes. Setting $a(x) = 0$ in ρ_B we find that the minimum corresponds to $f(x_{\min}) = \pi/2$. Splitting the

integral of the baryonic charge density into two parts,

$$B = \int_0^{x_{\min}} \rho_B dx + \int_{x_{\min}}^{\infty} \rho_B dx \quad (26)$$

we find for both parts the value $1/2$.

Let us next discuss the charge densities for $\eta_0 = 0.0001$. In this case we observe from Fig. 6 that the peaks of ρ_{MP} and ρ_B are roughly at the same location. However, at a large distance from these peaks the function ρ_{MP} possesses a second local maximum. We found, that the magnetic charge stems mainly from this second local maximum, whereas the contribution from the global maximum is marginal. This behaviour becomes plausible if we consider the profile of the gauge field function $a(x)$ in Fig. 4a. For small values of x the function $a(x)$ is close to one. Consequently, the magnetic charge density is small. For larger values of x the function $a(x)$ develops a local minimum, this leads to the first peak of ρ_{MP} . When $a(x)$ approaches again the value one, the function ρ_{MP} again becomes very small. At large distances the function $a(x)$ decays to its asymptotic value. This leads to the second maximum of ρ_{MP} . However, the magnetic charge density also depends on the Higgs field function $h(x)$, and one would expect that the charge density has to be small if $h(x)$ is small, i. e. in the region where the gauge field function possesses its local minimum, see Figs. 4a and 4b. This is indeed the case. Note, that for $\eta_0 = 0.0001$ the normalization constants of the function ρ_B is several orders of magnitude larger than the normalization constant of the function ρ_{MP} . Thus, the Monopole charge density at the first peak is indeed very small compared to the baryon charge density.

In analogy to the interpretation of a Monopole inside a baryon for large values of η_0 , one could interpret the solutions for small values of η_0 as a baryon inside a Monopole. However, the gauge field is nontrivial at the location of the baryon and the Higgs field is not in the vacuum in this region. Thus the baryon would reside in a nearly symmetric phase. One may speculate, that this scenario might be interesting in respect to the decay of the baryon.

4.3 $g_{\pi\Phi} > 0$

In most calculations we fixed the parameter $g_{\pi\Phi} = 0$. In view of the discussion in section 2 this needs some clarification. The interaction term of the chiral matrix with the Higgs field was introduced into the model basically for ideological reasons as it fixes the value of chiral function at infinity, $f_{\infty} = 0$ (say). Then we assumed that in the limit $g_{\pi\Phi} \rightarrow 0$ the asymptotic value of the chiral function is still fixed, and that the field configurations behave smoothly. Indeed, we found from our numerical analysis that this is the case and that the assumption is justified.

Let us now discuss the case where $g_{\pi\Phi}$ is finite. As long as $g_{\pi\Phi}$ is small, the dependence of the solutions on the parameters η_0 and κ does not change considerably. In particular the bifurcation pattern for small values of η_0 as shown in Figs. 3 persists for small $g_{\pi\Phi}$. The reason is simply that $g_{\pi\Phi}$ enters the differential equations only as a factor of the Higgs field function $h(x)$. In the limit $\eta_0 \rightarrow 0$ the Higgs field function vanishes and consequently the equations do not depend on $g_{\pi\Phi}$ in this limit. To discuss the more general case of finite η_0 let us assume that for some parameters κ, λ, η_0 solutions on the branches A, B and \tilde{A} coexist and form a butterfly in the $E - \eta_0$ diagram for $g_{\pi\Phi} = 0$. Then the butterfly will persist for small values of $g_{\pi\Phi}$. As $g_{\pi\Phi}$ increases, the butterfly shrinks in size and disappears at a critical value of $g_{\pi\Phi}$, e. g. $g_{\pi\Phi}^{cr} \approx 0.4$

for fixed $\kappa = 0.4$ and $\lambda = 0$. Thus, the bifurcation pattern is similar to Fig. 3, if we replace κ by η_0 , η_0 by $g_{\pi\Phi}$ and interchange the role of A and B .

We now consider the case where $g_{\pi\Phi}$ becomes very large at fixed parameters κ, λ, η_0 . In the limit $g_{\pi\Phi} \rightarrow \infty$ the potential (2) becomes a constraint, which for the spherically symmetric Ansatz (15), (16) becomes

$$h^2(x) \sin^2 f(x) \longrightarrow 0 \quad \text{as} \quad g_{\pi\Phi} \rightarrow \infty. \quad (27)$$

Note, that this constraint can neither be solved by a vanishing Higgs field function, $h(x) \equiv 0$, because this violates the boundary condition $h(x \rightarrow \infty) = \eta_0$, nor by a constant chiral function, $f(x) \equiv 0$ or π , because this violates boundary conditions at the origin or at infinity. However, there is a third possibility. If the Higgs field function vanishes on the interval $[0, x_0]$ and the chiral function vanishes on the interval $[x_0, \infty]$ then the function $h^2(x) \sin^2 f(x)$ vanishes everywhere.

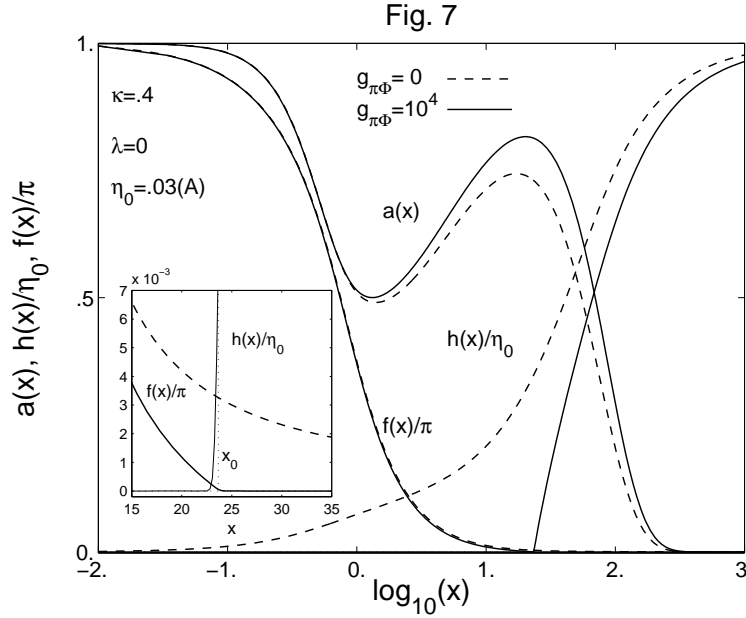


Figure 7: The profiles of the gauge field function $a(x)$, the scaled Higgs field function $h(x)/\eta_0$ and the scaled chiral function $f(x)/\pi$ are shown for $g_{\pi\Phi} = 10^4$ (solid lines) and $g_{\pi\Phi} = 0$ (dashed lines) for fixed $\kappa = 0.4$, $\lambda = 0$ and $\eta_0 = 0.03$ on the branch A .

In Fig. 7 we show the field configurations for $g_{\pi\Phi} = 10^4$ and for $g_{\pi\Phi} = 0$ for comparison for fixed parameters $\kappa = 0.4$, $\lambda = 0$ and $\eta_0 = 0.03$ on the branch A . We observe that the Higgs field function $h(x)$ is indeed almost zero on the interval $[0, x_0]$, with $x_0 \approx 23.65$, while the chiral

function $f(x)$ changes continuously from $f(0) = \pi$ to $f(x_0) \approx 0$. On the interval $[x_0, \infty]$ the chiral function is almost zero and the Higgs field function changes continuously from $h(x_0) \approx 0$ to its asymptotic value $h(\infty) = \eta_0$. The figure suggests that in the limit $g_{\pi\Phi} \rightarrow \infty$ the derivatives of the functions $h(x)$ and $f(x)$ will be finite but non-continuous at x_0 , whereas the gauge field function remains twice differentiable at x_0 .

Taking into account the behaviour of the functions for large $g_{\pi\Phi}$, we observe from the differential equation for the chiral function $f(x)$ (20), that the $\pi\Phi$ interaction term will be almost zero for $x < x_0$. Assuming that $h(x)$ increases linearly at x_0 , we find for large $g_{\pi\Phi}$ that for $x > x_0$ the chiral function decays exponentially with the exponent $\sim -g_{\pi\Phi}$. Hence, we find the following scenario. For $x < x_0$ the interaction of the Higgs field with the chiral field vanishes, whereas for $x > x_0$ the chiral field becomes increasingly massive. Consequently, the baryon is trapped inside the Monopole. On the other hand, because the magnetic charge density is proportional to the Higgs field, there will be (almost) vanishing Monopole density for $x < x_0$ for large $g_{\pi\Phi}$ and the Monopole is expelled from the baryon.

5 Normal modes

To show the instability of a solution of Eqs. (20) we determine the eigenvalues of the fluctuation matrix around that solution. The existence of a negative eigenvalue of a normalizable fluctuation mode indicates that a deformation of the solutions in the direction of this mode lowers its energy. Hence this solution can not be stable. Therefore, to show the instability of a solution, it is sufficient to find a normalizable fluctuation mode with negative eigenvalue. For the discussion of the normal modes we will adopt the methods discussed in Refs. [14, 15].

Here we consider only radial fluctuations around the solutions. We use the dimensionless coordinate x from the beginning. We introduce into the Ansatz small space-time dependent fluctuations $\Psi_\alpha(x)e^{i\omega t}$, $\alpha = a, b, c, h, f$,

$$\begin{aligned} a(x) &\rightarrow a(x) + \Psi_a(x)e^{i\omega t}, \\ b(x) &\rightarrow b(x) + \Psi_b(x)e^{i\omega t}, \\ c(x) &\rightarrow c(x) + \sqrt{2}\Psi_c(x)e^{i\omega t}, \\ h(x) &\rightarrow h(x) + \frac{\Psi_h(x)}{x}e^{i\omega t}, \\ f(x) &\rightarrow f(x) + \frac{\Psi_f(x)}{x}e^{i\omega t}, \end{aligned} \tag{28}$$

and expand the Hamiltonian and Lagrangian to second order in the fluctuation function Ψ_α . As we are interested in the fluctuations around the static solutions, we set $b \equiv 0$, $c \equiv 0$ and extremize the Lagrangian in the background of the functions a, h, f , i. e. whenever second derivatives of these functions appear, they are replaced by the right hand side of the differential equations (20).

The form invariance of the Ansatz (14)-(16), expressed by Eqs. (17), (18), reflects itself in the existence of normal modes with vanishing energy eigenvalue. These gauge zero modes obey the conditions

$$\Psi_a = 0, \quad \Psi_c = \frac{x}{\sqrt{2}} \left(\frac{\Psi_b}{a} \right)', \quad \Psi_h = 0, \quad \Psi_f = 0. \tag{29}$$

Because we are interested in the non-zero modes, we want to exclude the gauge zero modes. This can be done by imposing the conditions that the normal modes have to be orthogonal to the gauge zero modes with respect to the metric

$$< \tilde{\Psi}, \Psi >_{bc} = \int \left(\tilde{\Psi}_b \Psi_b + \tilde{\Psi}_c \Psi_c \right) + \dots \, dx . \quad (30)$$

(We will give the complete form of the metric later). This leads to the condition on the functions Ψ_b, Ψ_c

$$K[\Psi_b, \Psi_c] = (x\Psi_c)' - \sqrt{2}a\Psi_b = 0 . \quad (31)$$

To exclude the gauge zero modes we add μK^2 to the Lagrangian, where μ is a Lagrange multiplier.

From the system of differential equations we find, that the functions Ψ_b and Ψ_c couple to each other, but not to the functions Ψ_a, Ψ_h and Ψ_f and vice versa. Thus, we have two decoupled systems of differential equations, which can be solved separately.

5.1 The system $\{\Psi_b \Psi_c\}$

Let us first address the system $\{\Psi_b \Psi_c\}$. The differential equations become

$$\Psi_c'' + \omega^2 \Psi_c = 2 \frac{1+a^2}{x^2} \Psi_c + 2\sqrt{2} \frac{xa' - a}{x^2} \Psi_b , \quad (32)$$

$$\Psi_b'' + \omega^2 \Psi_b = V_{bb} \Psi_b + 2\sqrt{2} \frac{xa' - a}{x^2} \Psi_c , \quad (33)$$

and the corresponding static Hamiltonian is

$$\begin{aligned} \mathcal{H}_{bc}[\Psi_b, \Psi_c] = & \frac{4\pi f_\pi}{g} \int \left\{ V_{bb} \Psi_b^2 + \Psi_b'^2 + \frac{1+2a^2}{x^2} \Psi_c^2 + \Psi_c'^2 + 2 \frac{\Psi_c' \Psi_c}{x} \right. \\ & \left. + 2\sqrt{2} \left[\left(\frac{a}{x} \right)' \Psi_b \Psi_c - \frac{a}{x} (\Psi_b \Psi_c)' \right] \right\} dx \end{aligned} \quad (34)$$

with

$$V_{bb} = \left(\frac{3a^2 - 1}{x^2} + h^2 + \sin^2 f + 4\kappa^2 \sin^2 f \left(f'^2 + \frac{a^2 \sin^2 f}{x^2} \right) \right) , \quad (35)$$

where we have set the Lagrange multiplier μ equal to $\frac{1}{2}$. The boundary conditions for the functions Ψ_c and Ψ_b are given by

$$\begin{aligned} x = 0 & : \Psi_c = 0 , \Psi_b = 0 , \\ x \rightarrow \infty & : \Psi_c \rightarrow 0 , \Psi_b \rightarrow 0 . \end{aligned} \quad (36)$$

For solutions of (32), (33) we can evaluate the energy integral (34) by integration by parts and using (32), (33) and (36). We find for the dimensionless energy $E_{bc} = \frac{g}{4\pi f_\pi} \mathcal{H}_{bc}$,

$$E_{bc} = \omega^2 , \quad (37)$$

if we assume that the functions are normalised with respect to the metric (30). Thus, ω^2 denotes the energy eigenvalue in units of $4\pi f_\pi/g$.

We solved the system (32), (33) for several values of the parameters η_0 , κ , λ and $g_{\pi\Phi}$ and found only solutions with ω^2 positive. For fixed values of the parameters we found several discrete normal modes which can be characterized by the number of nodes N of the fluctuation function Ψ_b . Their eigenvalues ω_N^2 increase with the number of nodes N . The lowest positive eigenvalue ω_1^2 corresponds to one node of the function Ψ_b , see Fig. 8 (inlet). It seems to be likely that the system $\{\Psi_b\Psi_c\}$ possesses an infinite number of discrete positive eigenvalues, forming a sequence with convergence to η_0^2 .

	$\eta_0 = 0.032 \text{ (}\tilde{A}\text{)}$		$\eta_0 = 0.026 \text{ (}\tilde{A}\text{)}$	
N	$\omega_N^2 (\times 10^{-3})$	fit	$\omega_N^2 (\times 10^{-3})$	fit
1	0.9767	0.9608	0.66033	0.65785
2	1.0098	1.0080	0.67165	0.67144
3	1.0173	1.0169	0.67400	0.67400
4	1.0201	1.0200	0.67486	0.67486
5	1.0215	1.0214	0.67527	0.67527
6	1.0222	1.0222	0.67549	0.67549
7	1.0227	1.0227	0.67563	0.67563
8	1.0230	1.0230	0.67571	0.67571

Table 1

The eight lowest positive eigenvalues for $\eta_0 = 0.032$ and $\eta_0 = 0.026$ on the sphaleron branch \tilde{A} for $\kappa = 0.4$, $\lambda = 0$ and $g_{\pi\Phi} = 0$ together with the fitted eigenvalues.

For large N the eigenvalues ω_N^2 can be well approximated by the formula

$$\omega_N^2 = \left(\eta_0^2 - \frac{C}{N^2} \right)^2, \quad (38)$$

where C depends on the parameters η_0 , κ , λ and $g_{\pi\Phi}$. In Table 1 we give the first eight eigenvalues together with their fitted values for $\eta_0 = 0.032$ and $\eta_0 = 0.026$ on the branch \tilde{A} for fixed $\kappa = 0.4$, $\lambda = 0$ and $g_{\pi\Phi} = 0$. For the constants C we found $C(\eta_0 = 0.032) = 0.001$ and $C(\eta_0 = 0.026) = 0.00035$.

In Fig. 8 we show the lowest positive eigenvalue ω_1^2 as a function of η_0 for $\kappa = 0.4$, $\lambda = 0$ and

$g_{\pi\Phi} = 0$. For all branches B , A and \tilde{A} the eigenvalue is a monotonically increasing function of η_0 and vanishes in the limit $\eta_0 \rightarrow 0$.

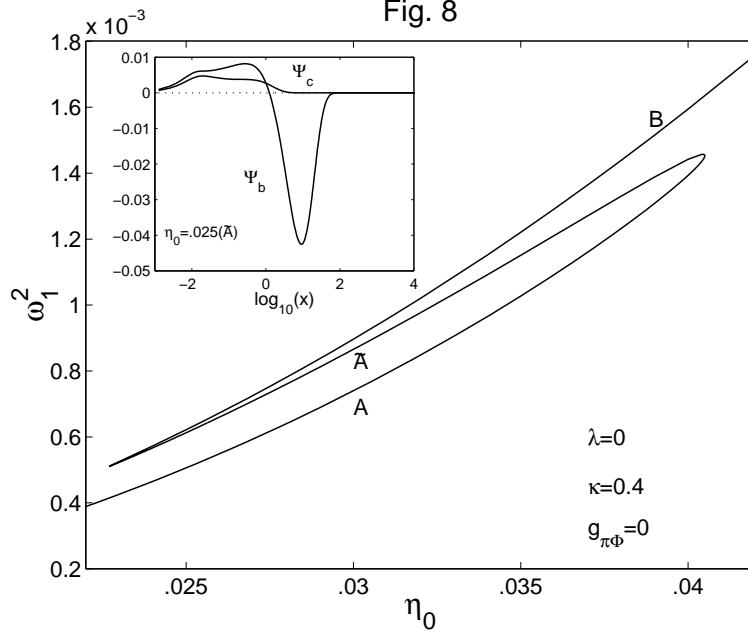


Figure 8: The lowest positive eigenvalue ω_1^2 is shown as a function of η_0 for fixed $\kappa = 0.4$, $\lambda = 0$ and $g_{\pi\Phi} = 0$. The inset shows the fluctuation functions $\Psi_b(x)$ and $\Psi_c(x)$ for $\eta_0 = 0.025$ on the branch \tilde{A} .

5.2 The system $\{\Psi_a \Psi_h \Psi_f\}$

For the system $\{\Psi_a \Psi_h \Psi_f\}$ the gauge zero modes are absent and we can calculate the differential equations and the static Hamiltonian directly. The system of differential equations is given by

$$\begin{aligned}
\Psi_a'' + \omega^2 \Psi_a &= \left[\frac{3a^2 - 1}{x^2} + h^2 + \sin^2 f + 4\kappa^2 \sin^2 f (f'^2 + \frac{3a^2 \sin^2 f}{x^2}) \right] \Psi_a \\
&+ \left[\frac{2ah}{x} \right] \Psi_h + \left[\frac{8\kappa^2 a f' \sin^2 f}{x} \right] \Psi_f' \\
&+ \frac{2}{x} \left[a \cos f \sin f + 4\kappa^2 a \sin f \left(\cos f f'^2 - \frac{\sin f f'}{x} + \frac{2a^2 \cos f \sin^2 f}{x^2} \right) \right] \Psi_f \quad (39)
\end{aligned}$$

$$\begin{aligned}
\Psi_h'' + \omega^2 \Psi_h &= \left[\frac{2a^2}{x^2} + g_{\pi\Phi}^2 \sin f + 4\kappa^2(3h^2 - \eta_0^2) \right] \Psi_h + \left[\frac{4ah}{x} \right] \Psi_a + \left[2g_{\pi\Phi}^2 \cos f \sin f h \right] \Psi_f \quad (40) \\
\Psi_f'' + \omega^2 \Psi_f &= \left[\frac{4}{xG} \left(a \cos f \sin f x^4 + 32\kappa^4 a^2 \sin^4 f (a^3 \cos f \sin f + a' f' x^2) \right. \right. \\
&\quad \left. \left. + 4\kappa^2 \sin f x^2 \left(2a^3 \cos f \sin^2 f - a \cos f f'^2 x^2 + 2a \sin f f' x - a' \sin f f' x^2 \right. \right. \right. \\
&\quad \left. \left. \left. - g_{\pi\Phi}^2 a \cos f \sin^2 f h^2 x^2 \right) \right) \right] \Psi_a \\
&\quad - \left[16\kappa^2 \frac{a \sin^2 f f' x}{8\kappa^2 a^2 \sin^2 f + x^2} \right] \Psi_a' + \left[2g_{\pi\Phi}^2 \frac{\cos f \sin f h x^2}{8\kappa^2 a^2 \sin^2 f + x^2} \right] \Psi_h \\
&\quad + \left[\frac{1}{x^2 G} \left(x^4 (2a^2 + g_{\pi\Phi}^2 h^2 x^2) (1 - 2 \sin^2 f) \right. \right. \\
&\quad \left. \left. + 64\kappa^4 a^3 \sin^2 f \left\{ a \sin^2 f (a^2 (1 - 2 \sin^2 f) - 2) + 2a \cos f \sin f f' x \right. \right. \right. \\
&\quad \left. \left. \left. + a f'^2 x^2 + 2a' x \sin^2 f \right\} \right. \right. \\
&\quad \left. \left. + 8\kappa^2 a x^2 \left\{ a \sin^2 f (a^2 (1 - 4 \sin^2 f) - 2) + 6a \cos f \sin f f' x + 2a \sin^2 f x^2 f'^2 \right. \right. \right. \\
&\quad \left. \left. \left. - a x^2 f'^2 - 4 \cos f \sin f a' f' x^2 + 2 \sin^2 f a' x - g_{\pi\Phi}^2 a \sin^2 f h^2 x^2 \right\} \right) \right] \Psi_f \\
&\quad + \left[\frac{16\kappa^2}{xG} a \sin f \left((x^2 + 8\kappa^2 a^2 \sin^2 f) (a (\sin f - \cos f f' x) - \sin f a' x) \right) \right] \Psi_f' \quad (41)
\end{aligned}$$

with

$$G = x^4 + 16\kappa^2 a^2 \sin f^2 (x^2 + 4\kappa^2 a^2 \sin f^2) . \quad (42)$$

We now find for the dimensionless energy of the solutions of the differential equations

$$E_{ahf} = \omega^2 \int \left\{ \Psi_a^2 + \frac{\Psi_h^2}{2} + \left[1 + \frac{8\kappa^2 a^2 \sin^2 f}{x^2} \right] \frac{\Psi_f^2}{2} \right\} dx . \quad (43)$$

From this form we can define an appropriate metric for the fluctuations Ψ by

$$\langle \tilde{\Psi}, \Psi \rangle = \int \left\{ \tilde{\Psi}_a \Psi_a + \tilde{\Psi}_b \Psi_b + \tilde{\Psi}_c \Psi_c + \frac{1}{2} \left(\tilde{\Psi}_h \Psi_h + \left[1 + \frac{8\kappa^2 a^2 \sin^2 f}{x^2} \right] \tilde{\Psi}_f \Psi_f \right) \right\} dx . \quad (44)$$

Assuming the normalisation of the fluctuation functions according to (44), we find the energy of the solutions to be $E_{ahf} = \omega^2$, i. e. ω^2 is again the energy eigenvalue.

For the system $\{\Psi_a \Psi_h \Psi_f\}$ we found normalizable solutions only on the saddlepoint branch \tilde{A} . For these normal modes the eigenvalue ω^2 is negative and vanishes at the bifurcation points. Hence these normal modes represent an instability mode of the saddlepoint solutions.

In Fig. 9 we show the negative eigenvalue ω^2 as a function of η_0 for $\kappa = 0.4$, $\lambda = 0$ and $g_{\pi\Phi} = 0$.

6 Summary and Discussion

We have studied a model combining the Georgi-Glashow and the Skyrme systems interacting mainly through the $so(3)$ gauge field, with an additional interaction term between the Higgs and

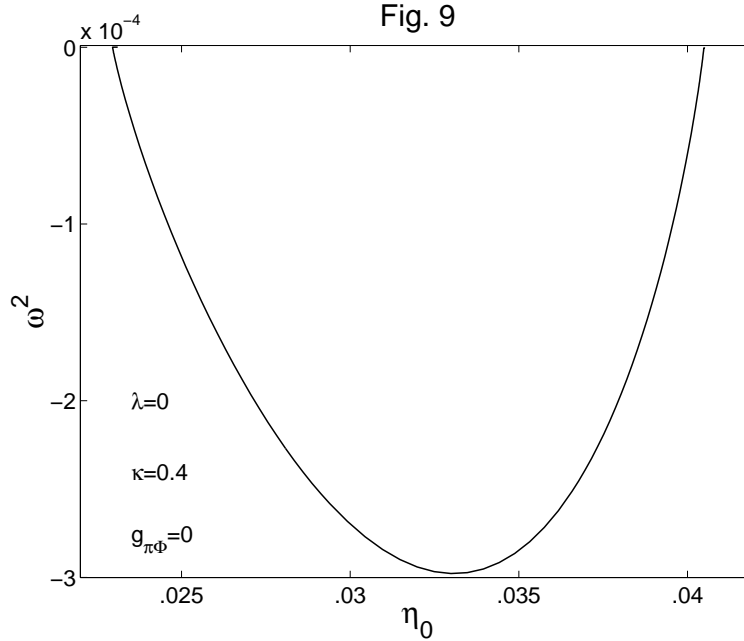


Figure 9: The negative eigenvalue ω^2 is shown as a function of η_0 for fixed $\kappa = 0.4$, $\lambda = 0$, $g_{\pi\Phi} = 0$.

chiral fields. This interaction term, which breaks the chiral symmetry and fixes the asymptotic value of the chiral field at infinity, exploits the non vanishing VEV of the Higgs field in an essential way.

The main emphasis of the study is the numerical analysis of the classical solutions of the model, which may be relevant to the semiclassical approach to monopole catalysis of Baryon decay [3]. The most interesting feature of these solutions, both intrinsically and for the physical reason just mentioned, is the particular bifurcation patterns that they exhibit. These patterns are connected to similar bifurcations in the solutions of the gauged Skyrme model, not involving a Higgs field, which has led us to make a systematic study of the relation between the solutions of these two models. This has been carried out by considering particular limits, in terms of the independent parameters involved in the Monopole-Skyrme model, in which the solutions of this model merge with the solutions of the Higgs independent gauged Skyrme model.

The above mentioned technical investigations form the centre of gravity of the present work. From the results obtained, some interesting observations of physical relevance can be made.

One is the particular shape of the bifurcations the solutions exhibit, namely what we have referred to as 'butterfly' in the text. These are reminiscent of the kind of bifurcations appearing in first order phase transitions. Unfortunately, in the present form of the model considered, we have not been able to make a concrete description for this phenomenon. This aspect of the work is under consideration.

The other observation can be made more quantitatively. It was shown that in some limit

of the parameters, the Baryon resides in the core of the monopole while in the other limit the converse, namely that the monopole resides inside the Baryon. In particular, for the values of the parameters fixed by the phenomenological values of the Higgs VEV and the pion decay constants, exactly one half of the Baryon charge resides inside the monopole core, and the rest outside.

Acknowledgements B. K. was supported by Forbairt grant SC/97-636; F. Z. was supported HEA postdoctoral fellowship.

References

- [1] V.A. Rubakov, JETP Lett **33** (1981) 658; "Theta-vacua, massless fermions and non-abelian magnetic monopoles", in: Problems of High Energy Physics and Quantum Field Theory. Proc. 4th Int. Seminar, Protvino, 1981. IHEP, vol. 1, p.148-155; Nucl. Phys. **B 203** (1982) 311.
- [2] C.G. Callan, Phys. Rev. **25** (1982) 2141; *ibid.* **D 26** (1982) 2058.
- [3] C.G. Callan and E. Witten, Nucl. Phys. **B 239** (1985) 161.
- [4] T.H.R. Skyrme, Proc. Roy. Soc. **A260** (1961) 127; Nucl.Phys. **31** (1962) 556.
- [5] G.'tHooft, Nucl. Phys. **B 79** (1974) 276; A.M. Polyakov, JETP Lett. **20** (1974) 194.
- [6] K. Arthur and D.H. Tchrakian, Phys. Lett. **B 378** (1996) 187.
- [7] Y. Brihaye and D. H. Tchrakian, Solitons/Instantons in d-dimensional SO(d) gauged O(d+1) dimensional Skyrme models, Nonlinearity **11** (1998) 891.
- [8] Y. Brihaye B. Kleihaus and D. H. Tchrakian, J. Math. Phys. **40** (1999) 1136.
- [9] B. Ratra and G. Yaffe, Phys. Lett. **B 205** (1988) 57;
- [10] T. Akiba, H. Kikuchi and T. Yanagida, Phys. Rev. D **38** (1988) 1937.
- [11] E. D'Hoker and E. Farhi, Nucl. Phys. **B 241** (1984) 109.
- [12] G. Eilam, D. Klabucar and A. Stern, Phys. Rev. Lett. **56** (1986) 1331.
- [13] V. A. Rubakov, Nucl. Phys. **B256** (1985) 509; J. Ambjorn and V. A. Rubakov, Nucl. Phys. **B256** (1985) 594.
- [14] T. Akiba, H. Kikuchi and T. Yanagida, Phys. Rev. D **40** (1989) 588.
- [15] Y. Brihaye, S. Giler, P. Kosinski and J. Kunz, Phys. Rev. D **42** (1990) 2846.